AGU PUBLICATIONS

JGR

Journal of Geophysical Research: Atmospheres

RESEARCH ARTICLE
10.1002/2016JD025115

Key Points:
- Two-year monitoring of AHs at six background sites across China's most developed regions
- Spatiotemporal patterns of compositions and sources of AHs were explored
- Ambient AH/CO ratios were compared with that in the emission inventory

Correspondence to:
Y. Zhang and X. Wang,
zhang_yl86@gig.ac.cn;
wangxm@gig.ac.cn

Citation:
Zhang, Z., Y. Zhang, X. Wang, S. Lü, Z. Huang, X. Huang, W. Yang, Y. Wang, and Q. Zhang (2016), Spatiotemporal patterns and source implications of aromatic hydrocarbons at six rural sites across China's developed coastal regions, *J. Geophys. Res. Atmos.*, *121*, 6669–6687, doi:10.1002/2016JD025115.

Received 12 APR 2016
Accepted 23 MAY 2016
Accepted article online 26 MAY 2016
Published online 14 JUN 2016

Spatiotemporal patterns and source implications of aromatic hydrocarbons at six rural sites across China's developed coastal regions

Zhou Zhang[1,2], Yanli Zhang[1], Xinming Wang[1,3], Sujun Lü[1,2], Zhonghui Huang[1,2], Xinyu Huang[1,2], Weiqiang Yang[1,2], Yuesi Wang[4], and Qiang Zhang[5]

[1]State Key Laboratory of Organic Geochemistry and Guangdong Key Laboratory of Environmental Protection and Resources Utilization, Guangzhou Institute of Geochemistry, Chinese Academy of Sciences, Guangzhou, China, [2]University of Chinese Academy of Sciences, Beijing, China, [3]Center for Excellence in Urban Atmospheric Environment, Institute of Urban Environment, Chinese Academy of Sciences, Xiamen, China, [4]Institute of Atmospheric Physics, Chinese Academy of Sciences, Beijing, China, [5]Ministry of Education Key Laboratory for Earth System Modeling, Center for Earth System Science, Tsinghua University, Beijing, China

Abstract Aromatic hydrocarbons are important anthropogenic precursors of tropospheric ozone and secondary organic aerosols. Here we measured ambient aromatic hydrocarbons from March 2012 to February 2014 at six rural sites in China's developed coastal regions. On average, benzene (B) comprised $>50\%$ of total benzene (B), toluene (T), ethylbenzene (E), and xylenes (X) (BTEX) at sites in the Northeast China Plain (NECP) or in the North China Plain (NCP), whereas T, E, and X accounted for $>77\%$ of total BTEX at sites in the Yangtze River Delta (YRD) and the Pearl River Delta in the south. BTEX at the northern sites was significantly correlated ($p<0.01$) with combustion tracer-carbon monoxide (CO) but weakly correlated with traffic marker-methyl tert-butyl ether (MTBE), suggesting that their main sources were coal and biofuel/biomass burning with substantially elevated B levels during the winter heating period. In contrast, BTEX at the southern sites originated mainly from traffic-related and/or industrial emission sources, as indicated by the poor correlations with CO but highly significant ($p<0.01$) correlations with MTBE and tetrachloroethylene, an industrial emission tracer. The B/CO emission ratios from measurement agreed within a factor of 2 with that of a previous widely used emission inventory of China, but the T/CO ratio at the NECP site and the o-X/CO ratio at the NCP site were 29% and 38% of that in the inventory, respectively; the E/CO and X/CO ratios at the YRD site were 3.2–3.5 fold that in the emission inventory.

1. Introduction

Aromatic hydrocarbons (AHs), including benzene, toluene, ethylbenzene, and xylenes (BTEX), are a class of volatile organic compounds (VOCs) that contribute substantially to nonmethane hydrocarbons in ambient air of urban areas [*Barletta et al.*, 2008; *Cai et al.*, 2010] and even in rural areas of China's developed regions [*Tang et al.*, 2009; *Zhang et al.*, 2014a]. AHs are emitted from a range of anthropogenic sources, such as fossil fuel combustion and solvent usage [*Chan et al.*, 2006; *Liu et al.*, 2008a; *Tsai et al.*, 2003; *Yuan et al.*, 2010a], as well as biomass burning [*Andreae and Merlet*, 2001]. As important precursors of tropospheric ozone [*Carter*, 1994; *Russell et al.*, 1995] and secondary organic aerosols (SOA) [*Forstner et al.*, 1997; *O'Dowd et al.*, 2002; *Odum et al.*, 1997; *Sato et al.*, 2010], AHs play an important role in photochemical smog and fine particle pollution, particularly in developed regions. For example, AHs contributed 35% and 54% to ozone formation potential in Beijing [*Wang et al.*, 2010] and Guangzhou [*Zou et al.*, 2015], respectively. As major anthropogenic precursors, AHs were responsible for $>75\%$ of secondary organic carbon in fine particles in the highly industrialized Pearl River Delta (PRD) region of southern China [*Ding et al.*, 2012; *Wang et al.*, 2013b]. The spatial distributions of SOA across six regions of China also suggested that AHs were the largest SOA contributor in northern China [*Ding et al.*, 2014]. Additionally, BTEX were identified as hazardous air pollutants: benzene is a known carcinogen that can cause leukemia, and other AHs may cause brain function disturbances and affect the heart and blood vessel system [*Agency for Toxic Substances and Diseases Registry*, 2009].

China's rapid urbanization and industrialization over the past three decades have resulted in increased air pollutant emissions (including BTEX) into the atmosphere [*Klimont et al.*, 2002; *Kurokawa et al.*, 2013; *Qiu et al.*, 2014; *Wei et al.*, 2014]. Anthropogenic emissions of AHs in China were estimated to be 4.4 Tg in 2005

and were expected to increase to 5.7 Tg by 2020 [*Wei et al*., 2008, 2014]. However, based on a comparison between satellite observations and model estimates of glyoxal vertical column densities, *Liu et al*. [2012] reported that the current emissions of AHs in China were significantly underestimated by a factor of 4–10, particularly in the developed regions of eastern China.

In situ observations could help constrain and reduce the uncertainties of air pollutant emission inventories [*Borbon et al*., 2013; *Hu et al*., 2015; *Wang et al*., 2014b], particularly when ambient measurements are conducted on large (regional or national) scales and over the long term. However, previous studies on ambient AHs in China were mainly carried out in a few metropolitan areas over short time periods, such as Beijing in summer [*Li et al*., 2014a; *Liu et al*., 2009; *Wang et al*., 2010, 2015b; *Zhang et al*., 2012a], Shanghai [*Cai et al*., 2010; *Wang et al*., 2013a, 2015a] and Guangzhou during the fall-winter [*Barletta et al*., 2008; *Liu et al*., 2008b; *Wang et al*., 2002; *Zhang et al*., 2013; *Zhao et al*., 2004]. These urban measurements are not representative of all developed regions, because the samples were collected at sites impacted mainly by emission sources on an urban scale, such as vehicle exhaust. Therefore, monitoring AHs at more background sites would reveal profound changes in their concentrations and composition in response to the changing spatiotemporal patterns of the emission sources. Although atmospheric VOCs have been investigated in several rural and remote regions, the measurements were obtained from a limited number of sites over short periods [*Guo et al*., 2004; *Suthawaree et al*., 2010; *Tang et al*., 2009; *Xue et al*., 2013; *Yuan et al*., 2013; *Zhang et al*., 2014a]. Field measurements of VOCs at background or remote locations remain scarce and sporadic in China. Several authors have reported VOC measurements at multiple sites, such as 45 cities in China for 2–5 days in January/February 2001 [*Barletta et al*., 2005], 84 sites in PRD for 4 days in 2008–2009 [*Louie et al*., 2013; *Zhang et al*., 2014b], 14 sites in southeast China for 10 days in 2011 [*Tong et al*., 2013], and 27 sites in Beijing during 16 days from July 2009 to January 2011 [*Wang et al*., 2014b]. However, these data do not provide a complete picture of VOCs on a regional or national scale due to the limited number of sampling days.

In this study, we monitored ambient AHs every Wednesday at six rural sites in China's developed coastal regions from March 2012 to February 2014 to determine their spatiotemporal variations in levels and composition. We further investigated the influence of the source regions using a backward trajectory analysis and explored their major emission sources from their relationship with typical source tracers. Finally, initial ratios of the individual components of BTEX to carbon monoxide (CO) were calculated based on ambient measurements and compared with those reported in a previous bottom-up emission inventory. This information would be helpful to formulate effective emission control strategies and improve estimates of China's emissions for these important anthropogenic VOCs.

2. Methods

2.1. Field Sampling

Field VOC samples were collected concurrently at six rural sites across China's most developed regions from March 2012 to February 2014 (Figure 1), including Hailun (HL) and Shenyang (SY) in the Northeast China Plain (NECP), Yucheng (YC) and Jiaozhou Bay (JZ) in the North China Plain (NCP), Taihu (TH) in the Yangtze River Delta (YRD) region, and Dinghushan (DH) in the Pearl River Delta (PRD) region. The sites are all ecosystem research stations included in the Chinese Ecosystem Research Networks, http://www.cern.ac.cn/0index/index.asp/). All sites are located in rural or remote areas with no factories or workshops, so the local anthropogenic emissions were unremarkable, and air pollutants originated mainly from surrounding cities. Therefore, they are suitable sites for monitoring regional atmospheric composition. Detailed descriptions of these rural sites are given below and in our previous study [*Zhang et al*., 2015].

The Hailun site (HL; 126.63°E, 47.43°N) is located in western Heilongjiang Province, 25 km southwest of Hailun City, 90 km northwest of Suihua City, and 180 km northwest of the provincial capital Harbin. Daqing City, a city known for the oil exploitation and petrochemical industry, is located 150 km southwest of the HL site. The sampling site is surrounded by farmland and small villages.

The Shenyang site (SY; 123.40°E, 41.50°N) is located in the center of Liaoning Province, which has long been a heavy industrial and mining center. The SY site is 35 km south of the provincial capital Shenyang, 38 km northwest of Benxi, 32 km northeast of Liaoyang, and 55 km northeast of Anshan. The sampling site is down wind of the surrounding industrial cities, making it a good regional monitoring station.

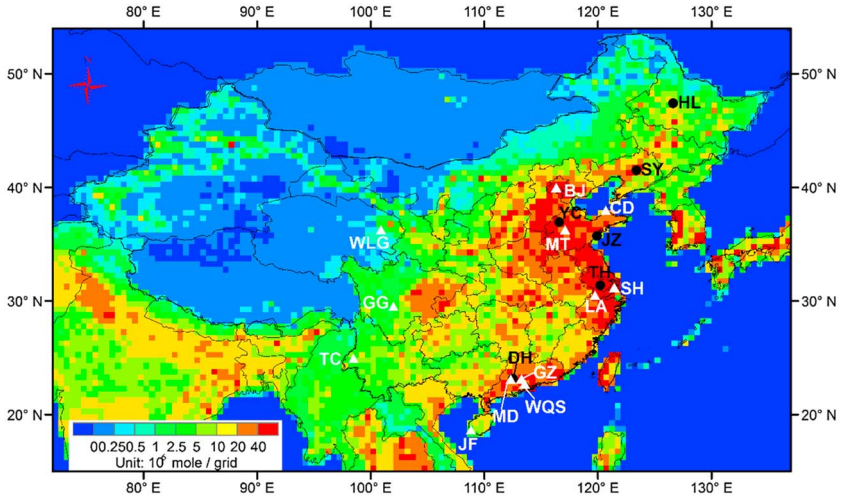

Figure 1. Locations of the sampling sites (black dots) across China's developed coastal regions. The white triangles indicate the sites for comparison in Table 1. The areas are color coded according to the emission strength of total BTEX from the anthropogenic emission inventory [*Li et al*., 2014b].

The Yucheng site (YC; 116.60°E, 36.95°N) is located in the NCP region, which geographically includes the municipalities of Beijing and Tianjin, Hebei and Shandong Provinces, and some parts of Shanxi and Henan Provinces. The YC site is 250 km southeast of the Beijing-Tianjin-Hebei region, and 56 km northwest of the provincial capital Jinan. The nearest city is Yucheng City, which is located 4 km east of the site. The sampling site is surrounded by farmlands and small villages.

The Jiaozhou Bay site (JZ; 119.93°E, 35.72°N) is a coastal site in southern Shandong Peninsula and adjacent to the west coast of the Yellow Sea. The JZ site is 55 km southwest of Qingdao City and 50 km northeast of Rizhao City. Influenced by the monsoon climate [*Zong et al*., 2016], the sampling site is often downwind of the continental area, particularly the NCP region.

The Taihu site (TH; 120.22°E, 31.40°N) is adjacent to the northeastern coast of Tai Lake in the YRD region, which has a typical southeast-northwest monsoon climate [*Cai et al*., 2010]. The TH site is 153 km southeast of Nanjing, 120 km west of Shanghai, and 120 km north of Hangzhou. The nearest city is Wuxi, which is located 15 km northeast of the site. Massive industrial point sources exist in the YRD region, such as iron and steel manufacturing, oil refining, and cement plants [*Fu et al*., 2013; *Li et al*., 2011].

The Dinghushan site (DH; 112.53°E, 23.17°N) is located in the northwest PRD region, which is one of the most important manufacturing centers in the world. The DH site is 18 km northeast of Zhaoqing City and 86 km west of the provincial capital Guangzhou. The site is on a hilltop in the Dinghushan National Natural Reserve with a total area of 11.55 km^2 of monsoon evergreen broad-leaved forests. The DH site is also included in the Baseline Air Pollution Monitoring Stations of the Chinese Academy of Sciences (http:www.cas.cn/zt/kjzt/ywtz).

Ambient air samples were collected at the six sites every Wednesday at approximately 14:00 local time. Ambient air was compressed into clean evacuated 1 L silonite-treated stainless steel canisters (Entech Instruments Inc., Simi Valley, California, USA) to approximately 200 KPa in approximately 60 min using a high-purity oil-free pump at a constant flow rate of 33 mL/min and controlled by a flow controller. A total of 561 samples were collected during the 2 year study, and the number of samples collected at each site is given in Table 1. These samples were transported back to the laboratory and analyzed within 1 month after collection.

2.2. Laboratory Analysis of VOCs and Carbon Monoxide

The air samples were analyzed with a model 7100 preconcentrator (Entech Instruments Inc., California, USA) coupled with an Agilent 5973 N gas chromatography-mass selective detector/flame ionization detector (GC-MSD/FID, Agilent Technologies, USA). Detailed cryogenic concentration steps are described elsewhere [*Wang and Wu*, 2008; *Zhang et al*., 2013]. In summary, 500 mL air samples were drawn through a liquid

Table 1. Mixing Ratios (pptv) of BTEX Measured in This Study and Comparison With Previous Studies in China

Site/Code	Sampling Period	N[a]	Benzene	Toluene	Ethylbenzene	m,p-Xylenes	o-Xylene	BTEX	Reference
					Rural Site				
Hailun/HL[b]	2012/03–2014/02	92	705 ± 207	231 ± 45	79 ± 12	169 ± 34	84 ± 16	1268 ± 247	This study
Shenyang/SY[b]	2012/03–2014/02	94	1220 ± 298	454 ± 76	153 ± 18	208 ± 28	101 ± 13	2136 ± 379	This study
Yucheng/YC[b]	2012/03–2014/02	99	1021 ± 185	485 ± 88	107 ± 18	98 ± 22	50 ± 10	1762 ± 286	This study
Jiaozhouwan/JZ[b]	2012/03–2014/02	94	515 ± 82	448 ± 83	166 ± 27	193 ± 31	94 ± 15	1417 ± 210	This study
Taihu/TH[b]	2012/03–2014/02	87	999 ± 158	2256 ± 387	1119 ± 211	819 ± 192	339 ± 66	5532 ± 847	This study
Dinghushan/DH[b]	2012/03–2014/02	95	615 ± 89	1262 ± 328	354 ± 91	327 ± 85	168 ± 41	2726 ± 562	This study
Changdao/CD[c]	2011/03–2011/04	-	990 ± 630	590 ± 480	160 ± 130	190 ± 210	70 ± 60	2000	*Yuan et al.* [2013]
Mount Tai/MT[c]	2006/06	30	641 ± 349	205 ± 123	61 ± 84	35 ± 73	81 ± 68	1023	*Suthawaree et al.* [2010]
Lin'an/LA[c]	2004/04–2004/05	83	750 ± 370	2640 ± 3000	330 ± 260	320 ± 260	150 ± 150	4190	*Tang et al.* [2009]
Mount Dinghu/MD[c]	2005/04	30	1170 ± 540	3090 ± 1790	480 ± 280	660 ± 480	270 ± 180	5670	*Tang et al.* [2007]
Wanqingsha/WQS[b]	2009/11–2009/12	74	1914 ± 247	5935 ± 800	1089 ± 145	740 ± 97	309 ± 42	9987	*Zhang et al.* [2013]
					Remote Site				
Mount Waliguan/WLG[c]	2003/04–2003/05	63	86 ± 47	184 ± 275	24 ± 40	120 ± 247	46 ± 81	460	*Xue et al.* [2013]
Mount Gongga/GG[c]	2008–2011	380	720 ± 640	440 ± 330	280 ± 420	280 ± 420	310 ± 430	2030	*Zhang et al.* [2014a]
Mount Tengchong/TC[c]	2004/04–2004/05	78	240 ± 70	160 ± 100	30 ± 40	60 ± 10	30 ± 50	520	*Tang et al.* [2009]
Mount Jianfeng/JF[c]	2004/04–2004/05	91	130 ± 90	170 ± 440	20 ± 20	40 ± 30	-	360	*Tang et al.* [2009]
					Urban Site				
Beijing/BJ	2014/10	240	1980	3310	1130	1010	710	8140	*Li et al.* [2015]
Shanghai/SH[c]	2007/01–2010/03	284	1810 ± 1190	4700 ± 4210	1230 ± 1020	1400 ± 1110	490 ± 360	9630	*Cai et al.* [2010]
Guangzhou/GZ[b]	2009/11–2009/12	69	2642 ± 265	4644 ± 544	786 ± 165	518 ± 93	226 ± 43	8816	*Zhang et al.* [2013]

[a]N indicates the number of samples.
[b]Values are average ±95% confidence interval.
[c]Values are average ± standard deviation.

nitrogen cooled cryogenic trap (0.32 cm × 20 cm) with glass beads (60/80 mesh) at −160°C. After trapping, this primary trap was heated to 10°C, and all target compounds were transferred by pure helium to the secondary trap (0.32 cm × 20 cm) at −50°C with Tenax-TA (60/80 mesh) as adsorbents. The redundant H_2O and CO_2 were mostly removed through this micropurge-and-trap step. The secondary trap was then heated to get VOCs transferred by helium to a third cryofocus trap (0.08 cm × 5 cm) at −170°C. After the focusing step, the trap was rapidly heated and the VOCs were transferred to the GC-MSD/FID system. The mixture was first separated by a DB-1 capillary column (60 m × 0.32 mm × 1.0 μm, Agilent Technologies, USA), with helium as the carrier gas at a constant rate of 4.0 mL/min, and then split into two ways controlled by a splitter to a 0.35 m × 0.10 mm I.D. stainless steel line output to MSD detection, and to a HP PLOT-Q column (30 m × 0.32 mm × 20.0 μm, Agilent Technologies, USA) output to flame ionization detector (FID) detection. The GC oven temperature was programmed to be initially at 10°C, held for 3 min; this then increased to 120°C at 5°C/min, and then to 250°C at 10°C/min with a final hold time of 20 min. The MSD was operated in selected ion monitoring mode and the ionization method was electron impacting (EI, 70 eV).

Carbon monoxide (CO) in the air samples was analyzed by an Agilent 6890 gas chromatograph equipped with an FID and a packed column (5 Å Molecular Sieve 60/80 mesh, 3 m × 0.32 cm). After separation by the packed column, CO was converted by a Ni-based catalyst to methane and was then detected by FID.

2.3. Quality Assurance and Quality Control

Before sampling, all canisters were cleaned at least 5 times by repeated filling and evacuating of humidified zero air. In order to check if there was any contamination in the canisters, all vacuumed canisters, after the cleaning procedure, were refilled with humidified zero air and stored in the laboratory for at least 24 h and then analyzed by the same methods as the field samples. A canister was labeled as a clean one if all the target VOC compounds were not present.

Target compounds were identified based on their retention times and mass spectra and quantified by external calibration methods. The calibration standards were prepared by dynamically diluting the Photochemical Assessment Monitoring Stations standard mixture and TO-15 standard mixture (100 ppbv, Spectra Gases Inc., New Jersey, USA) to 0.5, 1, 5, 15, and 30 ppbv, respectively. The calibration curves were obtained by running the five diluted standards, plus the humidified zero air, the same manner as the field samples. The

concentration response (peak area) correlation coefficients were 0.992–0.999. Each day, before sample analysis, the analytical system was checked initially with humidified zero air to ensure that it was clean and then with a one-point (typically 1 ppbv) calibration. If the response was beyond ±10% of the initial calibration curve, recalibration was performed. The measurement precision was determined by repeated analysis of a standard mixture (1 ppbv) seven times. The relative standard derivations for BTEX were all <5%. The method detection limits for benzene, toluene, ethylbenzene, m,p-xylenes, and o-xylene were 3 pptv, 5 pptv, 6 pptv, 9 pptv, and 6 pptv, respectively.

The analysis of methyl tert-butyl ether (MTBE) and tetrachloroethylene (C_2Cl_4) was the same as that of AHs. They were also identified based on their retention times and mass spectra and quantified by external calibration methods with the TO-15 standard mixture. CO was calibrated by one point standard (1 ppmv, Spectra Gases Inc., New Jersey, USA).

2.4. Calculation of Initial Mixing Ratios

The mixing ratios and composition of AHs change over time due to their different photochemical loss rates during transport from the emission source to the receptor site [*Borbon et al*., 2013; *de Gouw et al*., 2005; *Parrish et al*., 2007; *Warneke et al*., 2007]. In this study, the "OH exposure method" was applied to calculate the initial mixing ratio, as described by the following equation [*McKeen et al*., 1996; *Shao et al*., 2011; *Wang et al*., 2013a]:

$$[\mathrm{AH}_i]_t = [\mathrm{AH}_i]_0 \times \exp(-k_i[\mathrm{OH}]\Delta t) \tag{1}$$

$$[\mathrm{OH}]\Delta t = \frac{1}{k_\mathrm{X} - k_\mathrm{E}} \times \left(\ln\left\{ \frac{[\mathrm{X}]}{[\mathrm{E}]}\bigg|_{t=t_0} \right\} - \ln\left\{ \frac{[\mathrm{X}]}{[\mathrm{E}]}\bigg|_{t=t} \right\} \right) \tag{2}$$

where $[\mathrm{AH}_i]_0$ and $[\mathrm{AH}_i]_t$ are the initial and observed mixing ratios of AH_i, respectively, k_i is the reaction rate constant of AH_i with OH radicals, k_X and k_E are the reaction rate constant of m,p-xylenes (X) and ethylbenzene (E) with OH radicals, respectively [*Atkinson and Arey*, 2003], [OH] is the mixing ratio of OH radicals, Δt is the reaction time or photochemical age, $([\mathrm{X}]/[\mathrm{E}])_{t=t0}$ is the initial ratio of [X] to [E] in the emission source, and $([\mathrm{X}]/[\mathrm{E}])_{t=t}$ is the observed ratio of [X] to [E] at time t. The initial composition and ratio were calculated from the initial mixing ratio.

The ratio of [X] to [E] is widely applied to estimate photochemical age [*Shao et al*., 2011; *Wang et al*., 2013a; *Yuan et al*., 2013] because xylenes and ethylbenzene have similar sources and their emission ratios from different sources remain constant [*Liu et al*., 2008a; *Monod et al*., 2001; *Nelson and Quigley*, 1983]. Significantly strong correlations ($r = 0.84$–0.95, $p < 0.01$; Figure not shown) were found between m,p-xylenes and ethylbenzene at all sites in this study, suggesting similar sources. By inspecting various source profiles, we chose 2.2 pptv/pptv as the initial emission ratio of m,p-xylenes/ethylbenzene, which is comparable to the ratios in various local source profiles [*Liu et al*., 2008a] and in studies in Changdao (2.2) [*Yuan et al*., 2013], Beijing (2.0) [*Shao et al*., 2011], and Shanghai (2.0) [*Wang et al*., 2013a]. A sensitivity test showed that a ±0.5 pptv/pptv variation in the initial ratio of m,p-xylenes/ethylbenzene would induce −32% to 36% relative changes in the initial BTEX mixing ratios. Adding the measurement error (10%) produced calculated uncertainties in the initial BTEX mixing ratios within ±50%.

2.5. Backward Trajectory Analysis

Air pollutants contained in an air parcel at regional background or remote locations are largely influenced by the source regions through which they travel [*Jaars et al*., 2014; *Tang et al*., 2007, 2009; *Xue et al*., 2013; *Zhang et al*., 2014a]. Here the Hybrid Single-Particle Lagrangian Integrated Trajectory model (HYSPLIT, ver. 4.9; http://www.arl.noaa.gov/ready/hysplit4.html), developed by the National Oceanic and Atmospheric Administration (NOAA) Air Resources Laboratory (ARL), was applied to track air mass transport history [*Russo et al*., 2003]. The 72 h back trajectories arriving at 100 m above the ground level were computed once per sampling day at 14:00 local time (sampling time). These trajectories were further clustered by total spatial variance and grouping performance. A detailed description of the trajectory clusters is provided in section 3.3.

The boundary layer height was calculated at 14:00 local time on each sampling day using NOAA's READY Archived Meteorology online calculating program (http://ready.arl.noaa.gov/READYamet.php).

3. Results and Discussion

3.1. Ambient BTEX Levels

The BTEX mixing ratios (mean ± 95% confidence interval) observed in this study are listed in Table 1 and compared with those in previous studies. Notably, the observed VOC levels at the different sites were affected by sampling period, geographic location, meteorological conditions, chemical removal, and source emissions. Nevertheless, the comparison is helpful to provide an overview of the ambient BTEX levels in these areas.

Among the six rural sites, the total BTEX mixing ratio was the highest at the TH site in the YRD (5532 ± 847 pptv), followed by the DH site in the PRD (2726 ± 562 pptv), and was lowest at the HL site in the NECP (1268 ± 247 pptv) (Table 1). These results are consistent with the spatial distributions of anthropogenic BTEX emissions based on the bottom-up emission inventories (Figure 1) [*Li et al*., 2014b]. The mean values observed at the NECP and NCP sites in this study (1268 – 2136 pptv) were comparable with those observed previously at rural sites in the NCP, such as 2000 pptv at Changdao during March–April 2011 [*Yuan et al*., 2013] and 1023 pptv at Mount Tai in June 2006 [*Suthawaree et al*., 2010]. Total BTEX level at the TH site in the YRD was higher than 4190 pptv at Lin'an during April–May 2004 [*Tang et al*., 2009], which may have resulted from different sampling locations or periods as well as increasing anthropogenic emissions in the YRD [*Fu et al*., 2013]. In contrast, total BTEX at the DH site in the PRD was lower in the present study compared with that determined for Mount Dinghu during April 2005 (5670 pptv) [*Tang et al*., 2007] and Wanqingsha during November–December 2009 (9987 pptv) [*Zhang et al*., 2013]. This difference may be partly due to the longer distance from the emission source (compared with Wanqingsha), the higher boundary layer, and greater chemical removal at 14:00 local time, when the samples were collected in this study. Additionally, the observed levels at the six rural sites (1268 –5532 pptv) were much lower than those measured in Chinese megacities, such as 8140 pptv in Beijing during October 2014 [*Li et al*., 2015], 9630 pptv in Shanghai during 2007–2011 [*Cai et al*., 2010] and 11,267 pptv in Guangzhou during November–December 2009 [*Zhang et al*., 2013], but much higher than those in remote areas of China, such as 360 pptv on Mount Jianfeng during April–May 2004 [*Tang et al*., 2009], 460 pptv on Mount Waliguan during April–May 2003 [*Xue et al*., 2013], and 520 pptv on Mount Tengchong during April–May 2004 [*Tang et al*., 2009]. Measurement on Mount Gongga during 2008–2011 [*Zhang et al*., 2014a] showed a total BTEX level (2030 pptv) comparable to that of rural sites in the NCP, because this site is influenced by strong anthropogenic emissions in the Sichuan-Chongqing Region (Figure 1) [*Li et al*., 2014b].

Benzene levels at SY (1220 ± 298 pptv), YC (1021 ± 185 pptv), and TH (999 ± 158 pptv) were significantly ($p < 0.05$) higher than those at HL (705 ± 207 pptv), DH (615 ± 89 pptv), and JZ (515 ± 82 pptv). These observed mean values are comparable with those at rural sites in China's developed regions (641–1170 pptv) (except Wanqingsha), lower than those in megacities (1810–2642 pptv), but higher than those at remote sites (86–240 pptv) (except on Mount Gongga) (Table 1). Moreover, the mean annual benzene levels at the six rural sites (515–1220 pptv) were alarmingly higher compared with the levels (60–480 pptv) monitored in 28 United States cities [*Baker et al*., 2008]. For toluene, ethylbenzene, and xylenes, their largest levels were all observed at the TH site in the YRD (339 ± 66 pptv–2256 ± 387 pptv), followed by the DH site in the PRD (168 ± 41 pptv–1262 ± 328 pptv). These levels at TH and DH sites were significantly ($p < 0.01$) higher than those at sites in the NECP and NCP (50 ± 10 pptv–485 ± 88 pptv). In particular, the mixing ratios of ethylbenzene and xylenes at the TH site were comparable with those in Chinese megacities and much higher than those at the other rural and remote sites (Table 1).

3.2. Spatial Variation in Composition

As shown in Figure 2a, the observed BTEX composition varied with a distinct south-north contrast. At the northern sites of HL, SY, and YC, benzene was the most abundant among BTEX components and contributed 55.6%, 57.1%, and 54.6% to total BTEX, respectively. These proportions were more than twice those of toluene, which were only 23.1%, 21.3%, and 27.5%, respectively, at the three sites. In contrast, at the southern sites of TH and DH, toluene was the most abundant BTEX component, with proportions of 40.8% at TH and 46.3% at DH, which were more than twice those of benzene: 18.1% at TH and 22.6% at DH. However, the contributions of benzene (36.4%) and toluene (31.6%) to total BTEX at the JZ site were comparable, suggesting mixing of the two above-mentioned types. In addition, the contributions of C8-aromatics (sum of ethylbenzene, m,p-xylenes, and o-xylene) at TH (41.2%), JZ (32.0%), and DH (31.2%) were also higher than those at HL (24.6%), SY (21.6%), and YC (14.5%).

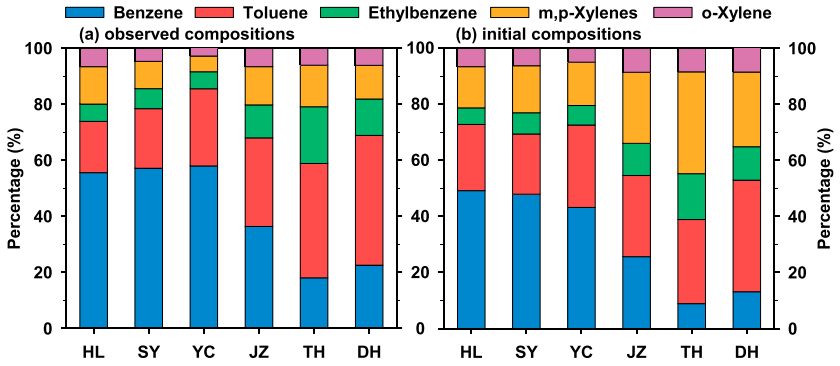

Figure 2. (a) Observed and (b) initial composition of BTEX at the six rural sites.

To eliminate the effect of photochemical aging on the observed BTEX proportions, we also compared the initial proportions of BTEX among the six rural sites (Figure 2b). Similar to the observed compositions, benzene was the most abundant of the initial BTEX components at the HL, SY, and YC sites, with contributions of 49.2%, 47.9%, and 43.2%, respectively. At TH site, m,p-xylenes were the largest contributor to initial BTEX (36.3%), followed by toluene (30.0%). At DH site, toluene was the dominant compound among initial BTEX (39.8%), followed by m,p-xylenes (26.6%). Indeed, the sum of toluene and C8-aromatics accounted for 91.1% and 86.9% of the initial total BTEX mixing ratios at the southern TH and DH sites, respectively, which were higher than those of 50.8%, 52.1%, and 56.8% at the northern HL, SY, and YC sites, respectively. At JZ site, the percentages of C8-aromatics in the initial proportions increased to 45.4%, compared with those in the observed proportions, whereas the percentages of toluene and benzene decreased to 29.0% and 25.6%, respectively. This "south-north" contrast in the observed and initial compositions of BTEX (Figure 2) from our long-term monitoring might reflect different emission sources.

3.3. Influence of Air Mass Transport

Figure 3 shows the representative trajectories of the air mass categories at each site and their corresponding initial mixing ratios and compositions of BTEX.

At the four northern sites—HL, SY, YC, and JZ (Figures 3a–3d), the lowest initial total BTEX mixing ratios (702 pptv–464 pptv) were all found in cluster #1 (12%–32% of periods), which originated from Siberia or Mongolia, quickly passed over the areas with little anthropogenic activity and low-density emissions, and arrived at the sites from the northwest in a fast descending motion. The highest initial total BTEX mixing ratios were all observed in clusters that had passed over areas with high-density emissions before arriving at the sampling sites. For example, cluster #2 at HL (1814 pptv; Figure 3a) passed over the nearest city (Hailun) around the site; cluster #2 at SY (3878 pptv; Figure 3b) received mainly outflow from the provincial capital city Shenyang; cluster #3 at YC (3175 pptv; Figure 3c) hovered over the low troposphere of southern Shandong Province with relatively stagnated air parcels; and cluster #3 at JZ (2615 pptv; Figure 3d) passed over the NCP region with high-density emissions [*Li et al*., 2014b; *Zhang et al*., 2009]. Benzene was the most abundant component in the initial BTEX composition in all clusters at the HL, SY, and YC sites, with contributions of 50.0%–58.0%, 36.4%–52.8%, and 37.7%–44.1%, respectively. At JZ site, toluene was the most abundant in all clusters with contributions of 27.8%–29.7%.

The initial total BTEX level in air masses arriving at TH (Figure 3e) in cluster #2 (16790 pptv) was higher than that in cluster #1 (10605 pptv) and #3 (10635 pptv). Air masses in cluster #2 originated from the lower troposphere of the East China Sea and passed over the YRD region (particularly the Shanghai metropolis), where more urban and industrial sources and high-density emissions of aromatics are found [*Fu et al*., 2013; *Huang et al*., 2011; *Li et al*., 2014b]. For all clusters, m,p-xylenes were the most abundant among the initial BTEX components, with contributions of 36.0%–36.5%. The sum of toluene and C8-aromatics contributed 91.2%, 92.2%, and 89.3% to initial total BTEX in clusters #1, #2, and #3, respectively. In particular, cluster #1 at TH, which originated from northern China, also showed high percentages of toluene and C8-aromatics, which differed from the initial proportions at the northern sites (HL, SY, and YC), where benzene was the dominant BTEX component. This occurred because cluster #1 passed over the northeastern part of Jiangsu

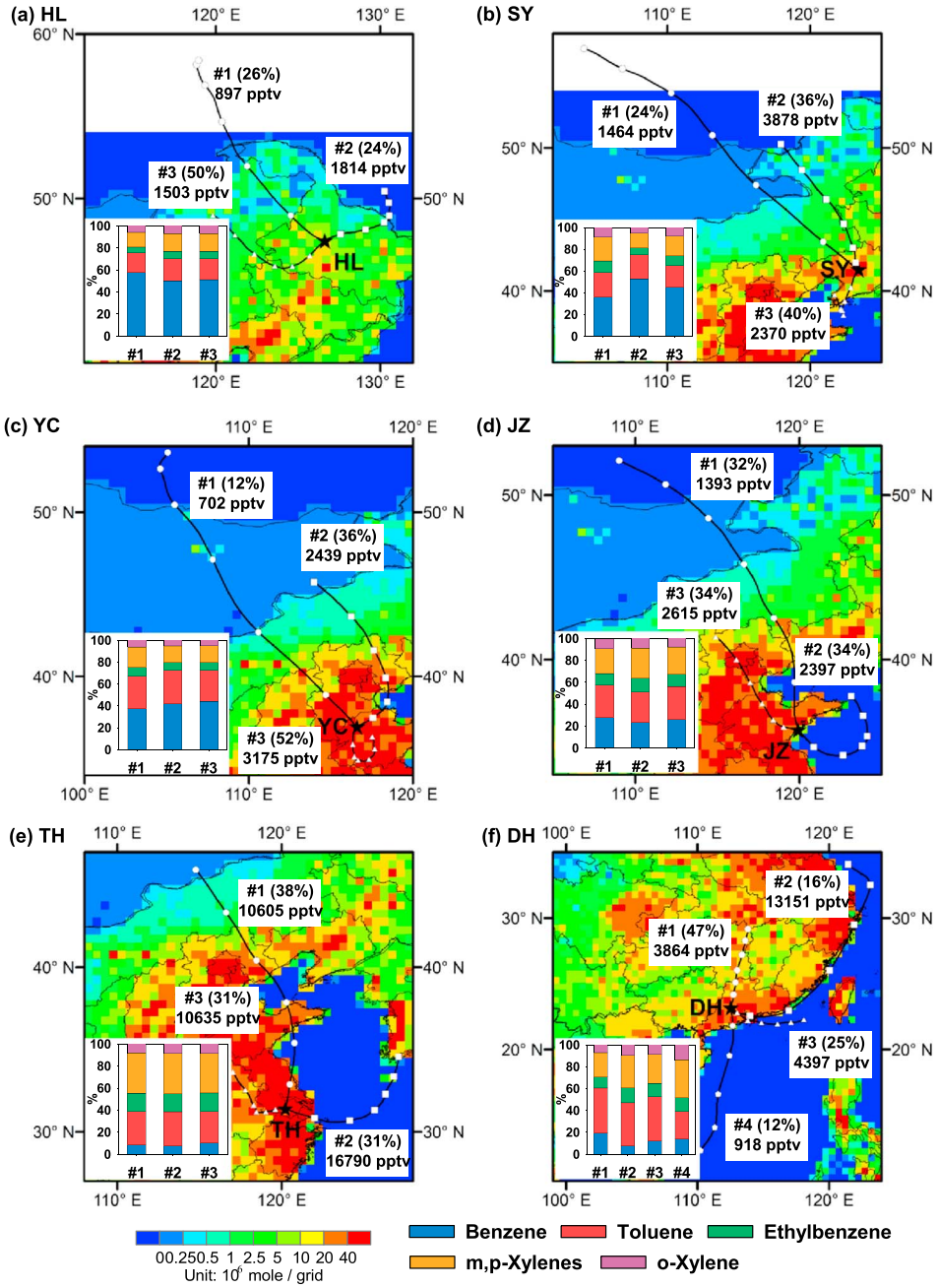

Figure 3. Initial compositions (inset bar chart) of BTEX for each cluster at the six rural sites. The percentages in parentheses refer to the frequencies in each cluster. Numbers below parentheses refer to the initial total BTEX mixing ratios (pptv).

Province and the nearest city (Wuxi), where emissions of toluene and C8-aromatics from industrial processes were very high [*Fu et al.*, 2013; *Huang et al.*, 2011].

Air masses arriving at DH were divided into four groups (Figure 3f). The cluster #2 (16%) air masses passed over the coast of southeast China and the central PRD region (e.g., Shenzhen, Dongguan, and Guangzhou) with high-density emissions [*Li et al.*, 2014b; *Zheng et al.*, 2009] and therefore showed the highest initial total BTEX mixing ratios (13151 pptv). In contrast, the air masses in cluster #4 (12%) had the lowest total BTEX (918 pptv), as they originated from the surface of the South China Sea and passed over the western part of Guangdong Province, bringing the cleanest air to the sampling site and diluting the pollutants. For initial compositions, m,p-xylenes were the most abundant component in cluster #4 (34.2%), whereas toluene

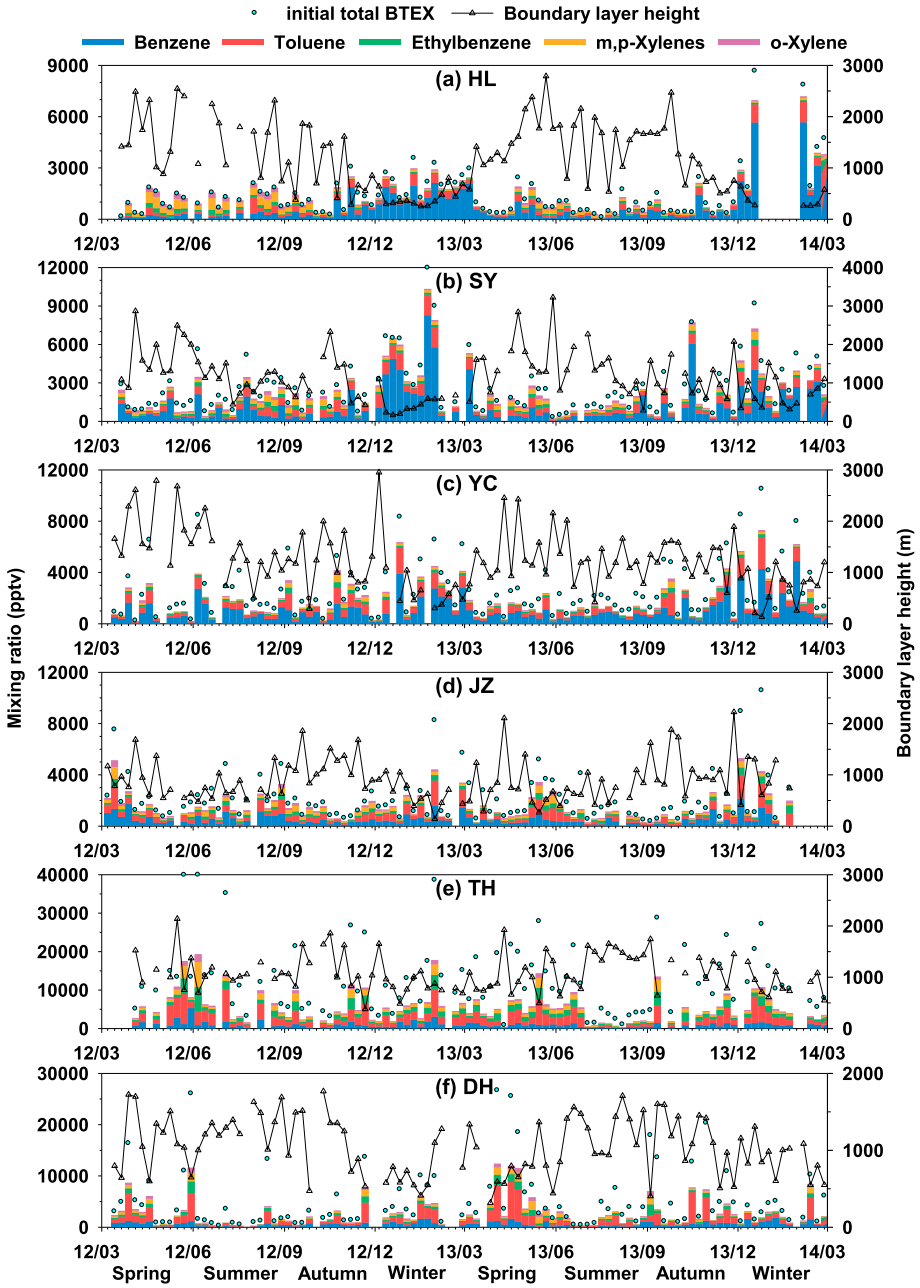

Figure 4. Temporal variations in the observed mixing ratios of BTEX (bar chart), initial total BTEX mixing ratios (circles), and boundary layer heights (triangles) at the six rural sites during the campaign. The minor ticks in *x* axis indicates the sampling day (every Wednesday).

was the most abundant in clusters #1–#3 (39.4%–40.7%). The total contributions of toluene and C8-aromatics to initial total BTEX ranged from 80.3% to 92.3% among the four clusters. In addition, the percentage of benzene in cluster #1 (19.7%) passing over central China and the northern part of Guangdong Province was higher than those in clusters #2–#4 (7.7%–14.2%).

3.4. Temporal Variations in Ambient Levels

Figure 4 shows the time series of observed BTEX mixing ratios at the six sites during the study, together with the initial total BTEX mixing ratios and boundary layer heights. At the HL site (Figure 4a), the observed total BTEX mixing ratios peaked on 18 December 2013 (6954 pptv) and 5 February 2014 (7108 pptv). Generally,

relatively high levels of total BTEX were observed during the winter of the 2 year study, largely due to increased benzene level. As shown in Figure 4a, benzene at HL exhibited low levels (235 ± 51 pptv) from mid-March to late October 2012 and 2013 (period I) but then increased and remained high (1506 ± 447 pptv) in the other periods (period II). The observed toluene mixing ratio varied similarly to that of benzene and increased from 163 ± 41 pptv during period I to 348 ± 91 pptv during period II. Several factors affecting the seasonal variations were further investigated, including chemical removal, boundary layer heights, source regions, and source emissions.

Slower chemical removal during winter would result in elevated levels. However, the initial total BTEX mixing ratio during period II (2343 ± 646 pptv) was also much higher than that during period I (878 ± 148 pptv) (Figure 4a), suggesting that chemical removal may not be the major reason for the elevated level during period II.

The lower boundary layer heights in winter could lead to an accumulation of pollutants in ambient air. As shown in Figure 4a, boundary layer height during period II (557 ± 112 m) was only approximately 36% of that during period I (1552 ± 149 m), which could partly explain the higher levels of BTEX during period II. However, the level of benzene during period II was more than sixfold that during period I. This is a much larger difference than that in the boundary layer height, suggesting that the higher benzene level during period II were also affected by other factors.

As for the variations in source regions, the percentages of clusters #1, #2, and #3 during period II were 29%, 47%, and 24%, which were similar to those during period I (24%, 52%, and 24%), respectively. Moreover, the initial total BTEX mixing ratios for clusters #1, #2, and #3 during period II were 1488 pptv, 3082 pptv, and 2508 pptv, which were all higher than those during period I (474 pptv, 1089 pptv, and 968 pptv), respectively. These results suggest that the increased BTEX level during period II was not induced by a difference in source region air masses passing through but rather was a regional phenomenon due to higher emissions.

Increased source emissions was another important factor causing the increased BTEX level during period II. In northern China, the domestic heating supply generally starts in mid-November and lasts until mid-March the following year. This heating period is longer in Heilongjiang Province due to longer periods of low temperatures. In 2012, 14.8% of coal consumption was used for heating in Heilongjiang Province, compared with 6.8% nationwide [*National Bureau of Statistics of China*, 2013]. Additionally, biofuel accounts for approximately two thirds of the total energy used for cooking and heating in China's rural areas [*Tang et al*., 2009; *Wei et al*., 2008; *Yan et al*., 2006], and the reported benzene emission factors of 25.8–1050 mg/kg for residential coal/biofuel combustion [*Tsai et al*., 2003] are extremely high compared with 0.59 mg/kg for controlled power plants and industrial coal combustion [*Garcia et al*., 1992; *United States Environmental Protection Agency*, 1995]. Therefore, the huge increase in coal and biofuel consumption for domestic heating could have increased the BTEX levels during period II, particularly the benzene levels.

Similarly, benzene and toluene mixing ratios at the other northern sites (Figures 4b–4d) during winter were 2631 ± 812 pptv and 808 ± 208 pptv at SY, 1776 ± 578 pptv and 753 ± 256 pptv at YC, and 758 ± 262 pptv and 717 ± 305 pptv at JZ, respectively, which were significantly ($p < 0.01$) higher than the mean mixing ratios of 763 ± 217 pptv and 340 ± 56 pptv at SY, 780 ± 129 pptv and 399 ± 77 pptv at YC, and 453 ± 76 pptv and 380 ± 67 pptv at JZ, respectively, observed during the other seasons. This increase during winter was caused primarily by additional source emissions, e.g., coal/biofuel combustion for heating, and/or low boundary layer heights. In contrast, the variation in C8-aromatics at the HL site was opposite to those of benzene and toluene. As shown in Figure 4a, the mean C8-aromatics mixing ratios at the HL site during April–October 2012 and 2013 was 429 ± 85 pptv, which was much higher than that (165 ± 45 pptv) during the other months, although a higher boundary layer height and faster chemical removal during April–October would decrease the ambient levels of C8-aromatics. Therefore, the increase in C8-aromatics observed at the HL site during April–October suggests increased emissions, most likely evaporative emissions due to higher temperatures during that period.

At TH site (Figure 4e), the mixing ratios of benzene, toluene, and C8-aromatics showed no significant seasonal variations ($p > 0.05$), although they tended to be higher in May 2012 and lower in August 2013. For example, mean C8-aromatics levels during spring, summer, autumn, and winter were 2555 ± 903 pptv, 2117 ± 1300 pptv, 2297 ± 854 pptv, and 2173 ± 705 pptv, respectively. Even for cluster #2 air masses (Figure 3e) arriving at TH from the east and passing over the highly industrialized YRD region (particularly the metropolis

Shanghai), the mean C8-aromatics mixing ratios in summer (2886 ± 3094 pptv) and winter (2838 ± 3378 pptv) were quite similar. The lack of significant seasonal variations in BTEX at TH was likely due to the constant industrial emissions over the year, which contribute major emissions of AHs to the TH site (section 3.5). For example, monthly industrial product only showed a relative standard deviation of 8% during 2013 in Shanghai in the YRD region (http://www.stats-sh.gov.cn/column/ydsj31/1.html). Faster chemical removal and higher boundary layer height during warmer seasons compared with cooler seasons would decrease ambient BTEX levels; however, more evaporative emissions in warmer seasons than cooler seasons would increase ambient BTEX levels. These counter effects would result in no significant seasonal variations in BTEX at the TH site. In addition, the effect of winter heating at the TH site may be minor due to the absence of central heat in this region, which is south of the great north-south central heating divide at the Qin-Huai line of China.

At DH site (Figure 4f), temporal variations of toluene and C8-aromatics peaked in April 2013, whereas benzene levels peaked in January 2013 and 2014. The toluene and C8-aromatics mixing ratios during spring were 2182 ± 960 pptv and 1619 ± 592 pptv, which is more than twofold higher than those during the other seasons (951 ± 278 pptv and 589 ± 170 pptv), respectively. However, the benzene mixing ratio was significantly lower ($p < 0.01$) during summer (262 ± 92 pptv) than that during the other seasons, but no significant differences ($p > 0.05$) were observed among spring (758 ± 185 pptv), autumn (591 ± 120 pptv), and winter (886 ± 226 pptv). Toluene, C8-aromatics, and total BTEX levels were also lowest in summer. These seasonal variations at the DH site could be explained by seasonal differences in source regions through which the air mass passed. Half of the air mass back trajectories during spring belonged to cluster #2 (Figure 3f), which passed over the coast of southeast China and the highly industrialized central PRD region (e.g., Shenzhen, Dongguan, and Guangzhou), with high densities of toluene and C8-aromatics emissions [*Li et al*., 2014b; *Zheng et al*., 2009]. This resulted in the higher levels of toluene and C8-aromatics during spring. The DH site was frequently affected by the cleanest air masses from the South China Sea during summer (cluster #4, Figure 3f), and the higher boundary layer height and faster chemical removal during summer may also have lowered BTEX levels (Figure 4f).

3.5. Source Implication

The characteristic ratios, such as toluene to benzene ratio, have been widely used to diagnose their sources in previous studies [*Barletta et al*., 2005, 2008; *Jaars et al*., 2014; *Tang et al*., 2009; *Zhang et al*., 2013]. Here we collected source profiles reported recently by different research groups [e.g., *Liu et al*., 2008a], including 28 examples from biomass burning, 35 examples from biofuel burning, 17 examples from coal burning, 11 examples from diesel vehicle exhaust, 31 examples from gasoline vehicle exhaust, 24 examples from gasoline evaporation, 25 examples from roadside or tunnel tests, and 66 examples from industrial processes and solvent applications. As shown in Figure 5a, despite several outliers, the toluene/benzene ratios were <1 for biomass/biofuel/coal burning, 1–10 for vehicle emissions, and >1 for industrial processes and solvent applications. *Barletta et al.* [2008] proposed a specific toluene/benzene ratio (>4.24) as indicator of the samples strongly affected by industrial emissions. However, this diagnostic value overlapped among different emission sources (Figure 5a).

In this study, the relative compositions of B, T, and E were plotted in a ternary diagram to better identify their sources (Figure 5b). As shown by the wireframes in Figure 5b, these profiles were grouped into three lumped source categories: (1) biomass/biofuel/coal burning, which is characterized by an extremely higher benzene fraction; (2) traffic emissions, which show high fractions of toluene, followed by benzene; this category includes profiles for diesel vehicle exhaust, gasoline vehicle exhaust, and gasoline evaporation, as well as results from roadside and tunnel tests; and (3) industrial processes and solvent applications, which are characterized by higher fractions of toluene and ethylbenzene, and a much lower fraction of benzene, as benzene has been forbidden in solvent use. The mean relative proportions of B, T, and E were 0.69:0.27:0.04 for biomass/biofuel/coal burning, 0.31:0.59:0.10 for traffic emissions, and 0.06:0.59:0.35 for industrial emissions, respectively.

The initial compositions of B, T, and E of each sample at the six rural sites are plotted in ternary diagrams (Figure 6). Figure 7 presents the mutual correlations between BTE and typical source tracers, including CO, a tracer of incomplete combustion of biomass/biofuel or fossil fuel [*Parrish et al*., 2009], methyl tert-butyl ether (MTBE), an exclusive indicator of traffic-related emissions [*Chang et al*., 2003], and tetrachloroethylene (C_2Cl_4), an industrial emissions marker [*McCulloch et al*., 1999; *Zhang et al*., 2012b].

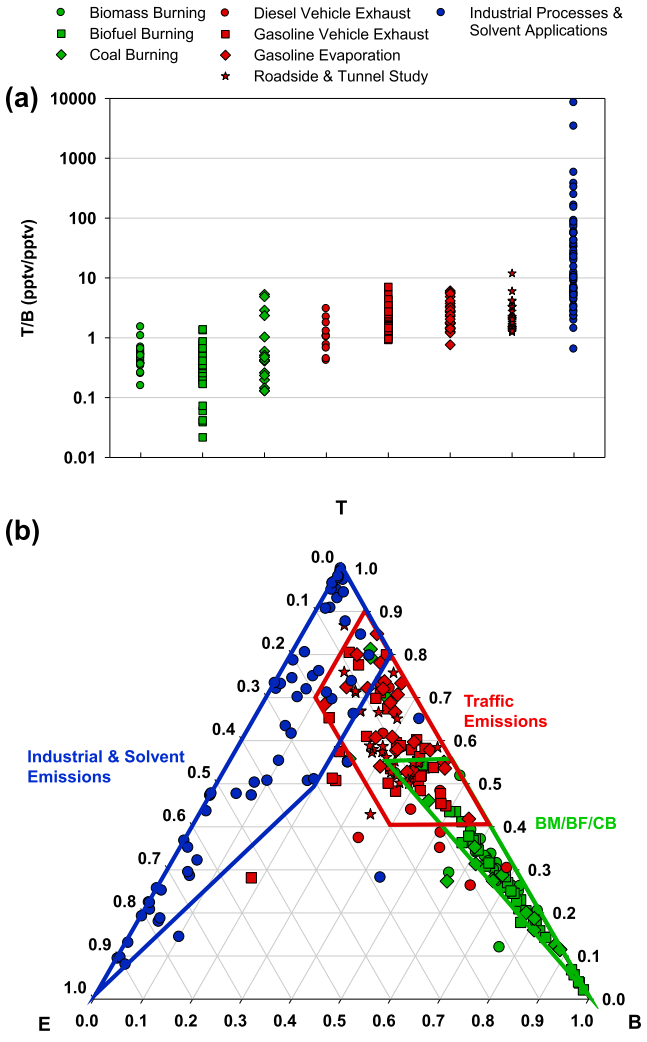

Figure 5. (a) Ratios of toluene to benzene (T/B) and (b) relative proportions of benzene (B), toluene (T), and ethylbenzene (E) in the source profiles of various sources. "BM/BF/CB" indicates biomass/biofuel/coal burning. The wireframes include more than 90% of the scatter collected for the three lumped source categories.

At the northern sites HL, SY, and YC, the proportions in most samples were scattered within or close to the composition scopes for biomass/biofuel/coal burning, with benzene as the dominant component (Figures 6a–6c). The initial benzene and toluene mixing ratio was significantly correlated with CO ($r > 0.66$, $p < 0.01$) but weakly correlated with MTBE ($r < 0.5$) (Figures 7a–7c), confirming that they were influenced more by the biomass/biofuel/coal combustion sources than by vehicle emissions at HL, SY, and YC sites. In particular, the initial proportions in the wintertime samples at these northern sites were concentrated in the scopes for biomass/biofuel/coal burning with a higher fraction of benzene (Figures 6a–6c), confirming the additional emissions of coal/biofuel combustion for wintertime heating. Figures 6a–6c also shows that some samples were scattered out of the source categories and had relatively high fractions of ethylbenzene, particularly samples taken during the warmer season at the HL site. The mean fraction of ethylbenzene observed at the three sites was higher (0.10–0.15), compared with the mean B:T:E ratio of 0.69:0.27:0.04 for biomass/biofuel/coal burning. The correlations between ethylbenzene and MTBE ($r = 0.58$ at SY) or C_2Cl_4 ($r = 0.53$ at HL and $r = 0.65$ at YC, respectively) suggest an impact from vehicle or industrial emissions. However, smaller slopes of ethylbenzene against MTBE and C_2Cl_4 at the three sites than those at TH and DH (Figure 7) suggests that the impact of vehicle or industrial emissions at HL, SY, and YC sites was less significant.

At TH site (Figure 6e), higher fractions of toluene (mean, 0.51) and ethylbenzene (0.32) relative to benzene (0.17) were detected, and most samples were scattered within or close to the scopes for industrial processes and solvent use. The poor correlation between toluene or ethylbenzene with CO ($r < 0.3$) and the significant correlation with C_2Cl_4 ($r > 0.6$, $p < 0.01$; Figure 7e) suggest a strong effect of industrial processes and solvent use at the TH site. Consistently, emission inventories also reported that industrial processes and solvent use were the main sources of aromatics in the YRD region [*Fu et al.*, 2013; *Huang et al.*, 2011].

The ternary plot for samples at the DH site (Figure 6f) revealed that the relative proportions of B, T, and E were scattered mostly in the regions of traffic-related emissions, industrial processes, and solvent use. This was also confirmed by the significant ($r > 0.5$, $p < 0.01$; Figure 7f) correlations between B, T, and E with MTBE and C_2Cl_4. In addition, the strong correlation between benzene and CO ($r = 0.81$, $p < 0.01$) and the lack of a correlation between toluene and CO ($r = 0.40$) or ethylbenzene and CO ($r = 0.29$) suggest that benzene at DH originated mainly from traffic-related emissions, whereas TEX were mainly emitted from industrial processes and solvent use. This was consistent with the positive matrix factorization source attributions of aromatics at four

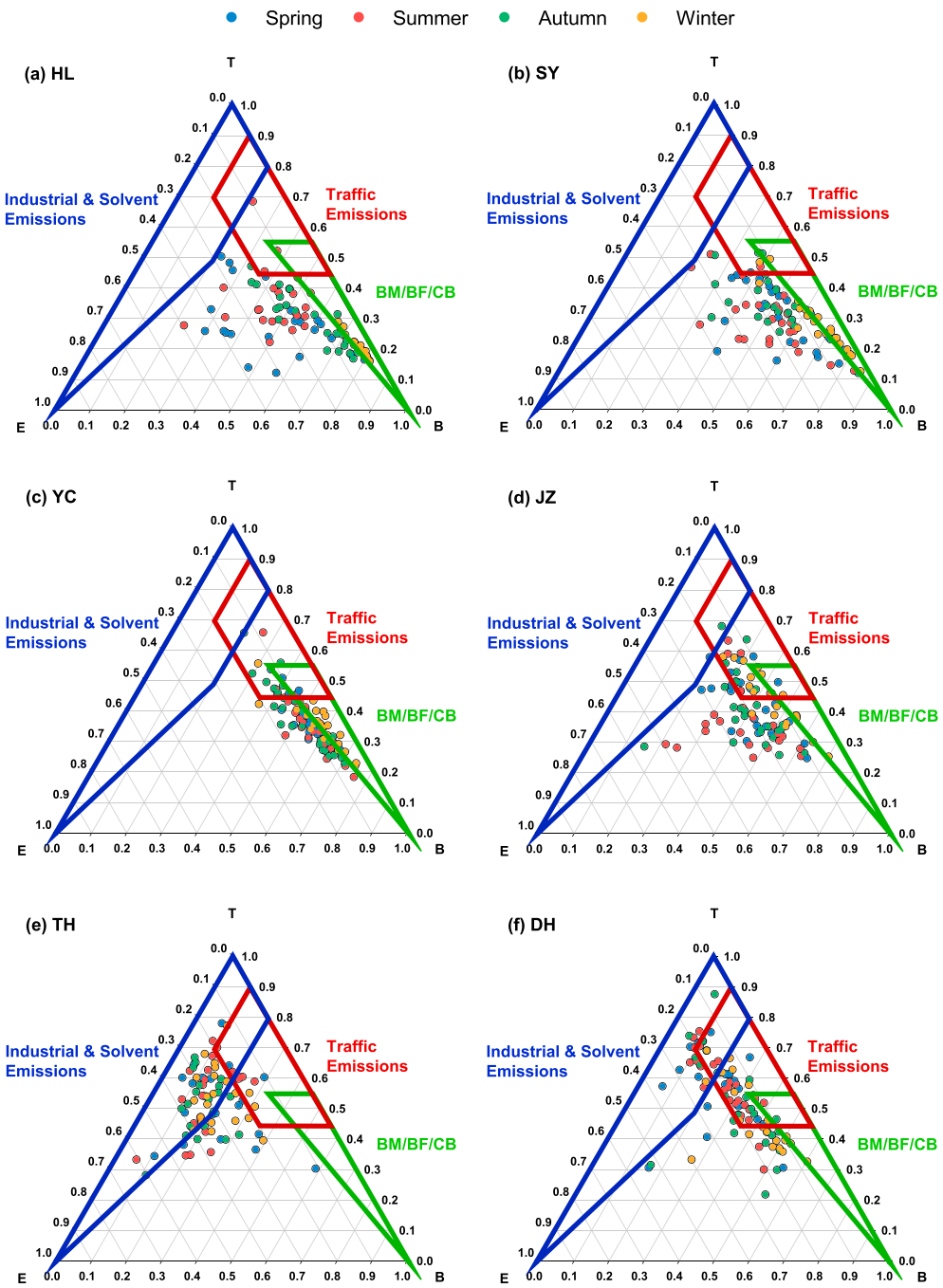

Figure 6. Initial proportions of benzene (B), toluene (T), and ethylbenzene (E) at the six sampling sites during different seasons.

representative sites in the PRD region [*Zhang et al.*, 2013], which revealed that vehicle exhaust was the major source of benzene, contributing 43–70%, whereas solvent use contributed 47–59% and 52–59% of toluene and C8-aromatics, respectively. A speciated VOC emission inventory for the PRD region also concluded that benzene originated primarily from traffic-related emissions (45%), whereas toluene originated mainly from industrial solvents (47.5–51.8%) [*Ou et al.*, 2015; *Zheng et al.*, 2009]. In the B, T, and E ternary plot for the DH site (Figure 6f), more samples in spring were scatters within the scope for industrial emissions with a higher ethylbenzene fraction. This finding is consistent with the above discussion that air masses in spring passed mainly over the highly industrialized central PRD region before arriving at the DH site.

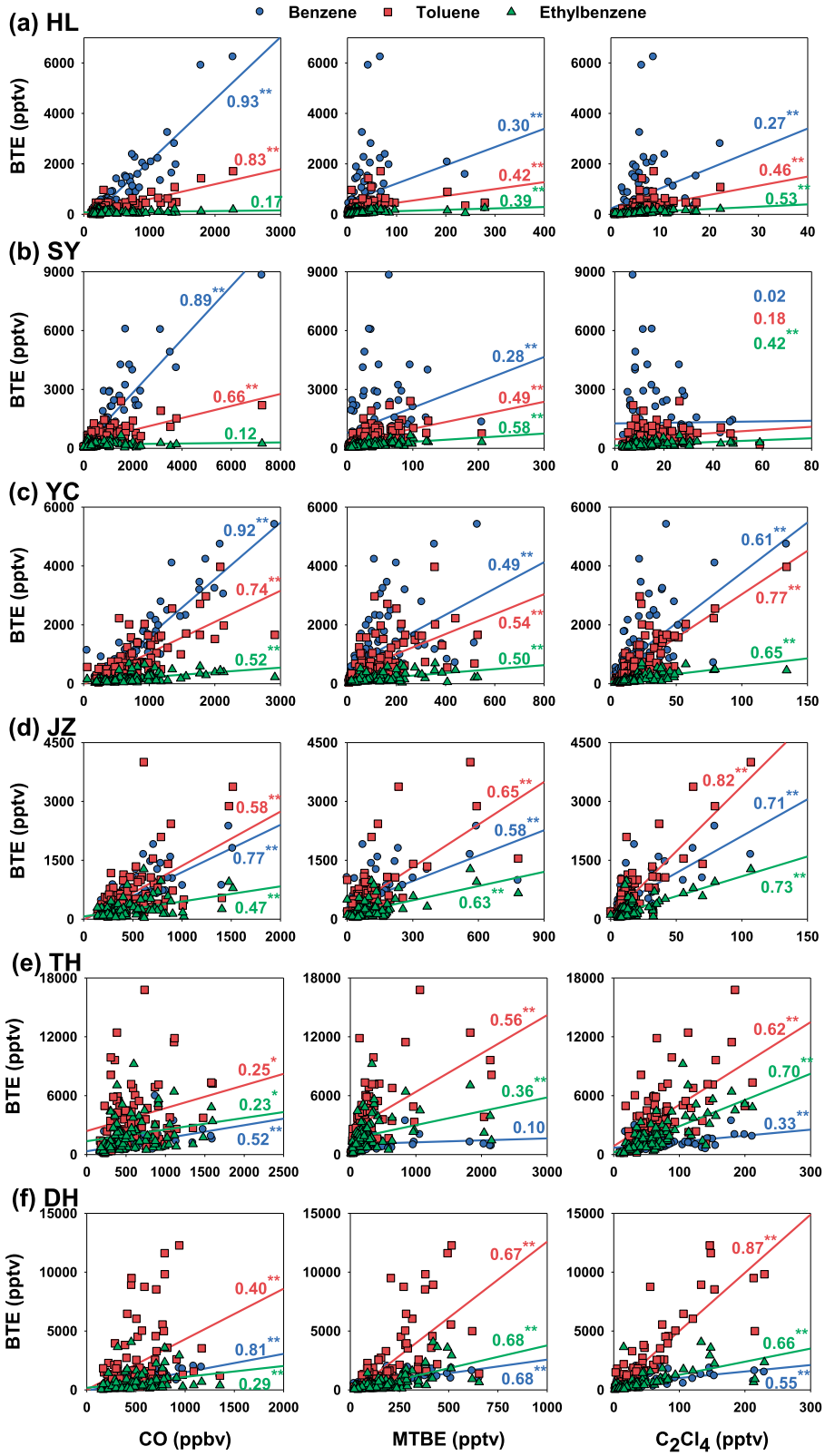

Figure 7. Correlation analysis of initial mixing ratios between BTE–benzene, toluene, and ethylbenzene, and typical tracers–carbon monoxide (CO), methyl tert-butyl ether (MTBE), and tetrachloroethylene (C_2Cl_4), at the six sampling sites during the study. The number near the regression line is the correlation coefficient (r), ** indicates r values with $p < 0.01$, * indicates r values with $p < 0.05$, and the nonstarred slopes indicate r values with $p > 0.05$.

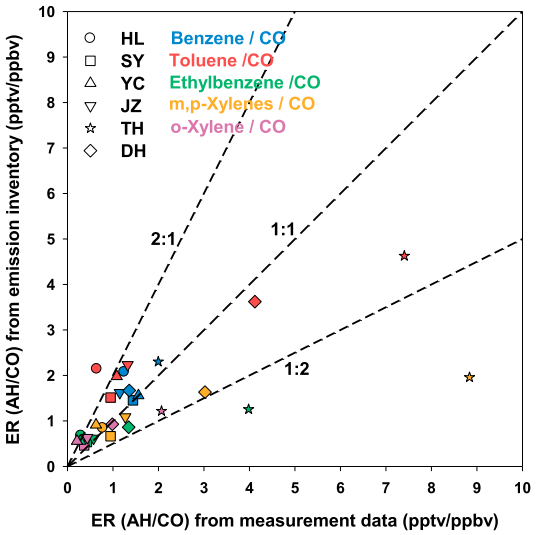

Figure 8. Comparisons of emission ratios of AHs to CO determined from measurement data with those from emission inventory data.

The ternary fractions of B:T:E at the JZ site averaged 0.41:0.41:0.18 and samples were scattered in the ternary plot (Figure 6d) without centering in any of the three source categories. The correlation analysis (Figure 7d) showed significant correlations ($r > 0.5$, $p < 0.01$) between aromatics (B, T, and E) and the tracers (CO, MTBE, and C_2Cl_4). This result suggests that BTEX at the JZ site were influenced by mixed emission sources. In addition, wintertime samples were mainly within the scopes of traffic emissions and biomass/biofuel/coal burning (Figure 6d), suggesting the importance of these combustion sources during winter at JZ site.

3.6. Evaluation of Anthropogenic Emission Inventory

Comparison of emission ratios of individual AHs relative to CO determined from field measurements with those from emission inventories is helpful to evaluate and validate current inventories [*Borbon et al.*, 2013; *Wang et al.*, 2014b; *Warneke et al.*, 2007; *Yuan et al.*, 2013]. The speciated AH emissions databases considered here are based upon the INTEX-B Asian anthropogenic emission inventory, which is the most widely used "bottom-up" inventory for China [*Li et al.*, 2014b; *Zhang et al.*, 2009]. Emissions in the 2.5°×2.5° regions with the central grid located at the sampling site were integrated for comparison, because the field measurements were made at receptor sites and influenced by the larger surrounding domains.

Figure 8 shows the scatterplots of the initial BTEX/CO ratios from our field measurements against those based on the emission inventory. The benzene to CO ratios in the emission inventory agreed within a factor of 2 with the initial ratios from the field measurements at all sites. However, there were some discrepancies for toluene and C8-aromatics. The toluene to CO ratio in the inventory was 3.4-fold the initial ratio from our measurements at the HL site; the o-xylene to CO ratio in the inventory was 2.6-fold the initial ratio from our measurements at the YC site; the ratios of ethylbenzene and m,p-xylenes to CO in the inventory were only 31% and 22%, respectively, of the initial ratios from our measurement at the TH site. On the other hand, the o-xylene to CO ratio at TH and the ratios of ethylbenzene and m,p-xylenes to CO at DH were near 1:2 (Figure 8). In addition, the inventory showed that the industrial sector (mostly noncombustion emissions) contributed 53.8% to toluene for the region around HL and 22.8% to o-xylene for the region around YC [*Li et al.*, 2014b], which was inconsistent with our measurements that aromatics at HL and YC were emitted mainly from combustion sources (section 3.5). While at TH site, the inventory revealed that industrial sector contributed only 24.6% and 24.1% of ethylbenzene and m,p-xylenes, respectively [*Li et al.*, 2014b]; however, our measurements suggested that industrial and solvent emissions were the most important sources for ethylbenzene and m,p-xylenes (section 3.5). These results suggest that emissions from the industrial sector in the inventory are probably overestimated for northeast China and the NCP but underestimated for the YRD region.

The uncertainties in the emission inventory and the limitations of the "top-down" approach based on ambient measurements could have caused the discrepancies in the BTEX to CO ratios. *Li et al.* [2014b] reported that source profiles are the most important source of uncertainties in emission estimates for individual nonmethane volatile organic compounds (NMVOC). Figure 9 compares the relative compositions of B, T, and E in the composition profiles used for the anthropogenic emission inventory by *Li et al.* [2014b] with those in various source profiles measured (Figure 5b). Except for a few outliers, the composition profiles of biofuel/coal burning and diesel/gasoline vehicle exhaust are located mainly within the wireframes for the corresponding source categories, suggesting that the profiles used in the inventory are reasonable. The outliers included diesel emissions from off-road transportation, coal burning from industrial combustion,

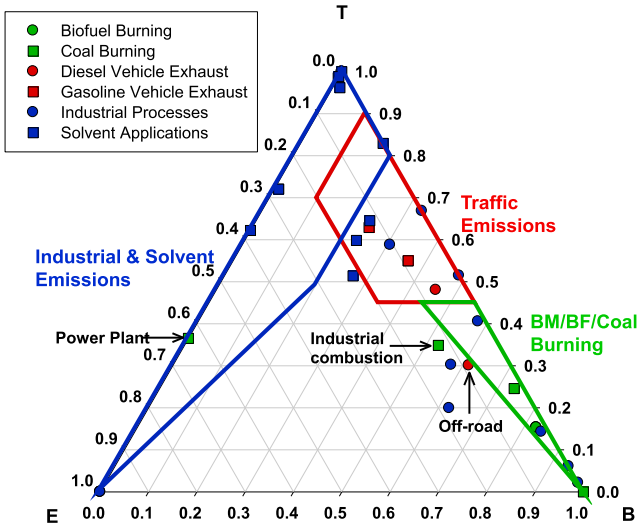

Figure 9. Relative proportions of benzene (B), toluene (T), and ethylbenzene (E) in the "composite" profiles used for the anthropogenic emission inventory [*Li et al.*, 2014b].

and coal burning from the power sector. However, due to their minimal contributions (3.2%, 3.1%, and 2.1%, respectively) to total NMVOC emissions [*Li et al.*, 2014b; *Zhang et al.*, 2009], these outliers probably had little effect on the speciated emission inventory. In contrast, Figure 9 demonstrates that the composition profiles for industrial processes and solvent applications used in the inventory were quite different from those measured in recent studies [e.g.,*He et al.*, 2015; *Tang et al.*, 2014; *Wang et al.*, 2014a; *Yuan et al.*, 2010a; *Zheng et al.*, 2013]. Local profiles are not available for many industrial categories, and those used to compile the inventory were mostly from the United States Environmental Protection Agency's SPECIATE database, which are measured mainly in the U.S. [*Simon et al.*, 2010] and may not accurately represent the chemical characteristics of sources in China [*Zheng et al.*, 2009]. This partly explained the large discrepancies in TEX, which had larger contributions from industrial processes and solvent use than those of benzene [*Liu et al.*, 2008a; *Yuan et al.*, 2010a; *Zheng et al.*, 2013]. In fact, the diverse and complex profiles among different solvents and various industrial processes (Figure 5) themselves cause huge uncertainties and difficulties estimating their emissions. Hence, more comprehensive and updated source characterization for industrial processes and solvent use are required to narrow the uncertainty of the emission estimates. In addition, the limitations of emission ratios based on ambient measurements should also be noted. In this study, annual mean emission ratios were used for comparison, which limits the temporal representation of VOC measurements lasting >1 year. It should also be noted that field measurements can be affected by open burning of biomass, particularly during harvest periods [*Suthawaree et al.*, 2010; *Yuan et al.*, 2010b], which also adds uncertainty when compared with anthropogenic emission inventories.

4. Conclusions

We measured atmospheric AHs for 2 years at six rural sites over developed coastal regions of China. The levels of toluene and C8-aromatics at the southern TH and DH sites were significantly higher than those at the northern HL, SY, YC, and JZ sites. The analysis of spatial differences in composition showed that benzene was the most abundant BTEX at HL, SY, and YC, whereas toluene was the most abundant at TH and DH. The backward trajectory analysis indicated that BTEX levels at these sampling sites were significantly higher in air masses that had passed over source regions with high-density emissions. The analysis of temporal variations in BTEX revealed increased benzene and toluene levels during winter at the northern sites, which was primarily caused by additional coal/biofuel combustion emissions for heating and/or low boundary layer heights. Additionally, no significant seasonal variations in BTEX were observed at the TH site, whereas the seasonal BTEX variations at DH were attributed to seasonal differences in air mass transport. Our results suggest that sites in northern China were affected mainly by biomass/biofuel/coal burning, whereas sites in southern China were affected mainly by traffic-related emissions and/or industrial emissions. These findings suggest the necessity of regionally and seasonally tailored control strategies to reduce BTEX levels and to mitigate their environmental impact and health effects.

Finally, the comparisons of AHs/CO emission ratios in the field measurement with those in the emission inventory suggested that the inventory may estimate benzene well but that toluene and o-xylene were overestimated in northeast China and the NCP, respectively. Furthermore, C8-aromatics were underestimated in the YRD region. Discrepancies in the source profiles of industrial processes and solvent applications between the inventory and local measurements may be an important source of the uncertainty.

Acknowledgments

The authors duly acknowledge the tremendous efforts of all the technicians involved in the field sampling. This study was supported by Strategic Priority Research Program of the Chinese Academy of Sciences (grant XDA05100104/XDB05010200/KJZD-EW-TZ-G06-03) and Natural Science Foundation of China (grant 41530641/41571130031/41121063). The suggestions of anonymous reviewers have greatly improved the quality of this manuscript and are sincerely appreciated. The authors also gratefully acknowledge the NOAA Air Resources Laboratory (ARL) for the provision of the HYSPLIT transport and dispersion model and the READY Archived Meteorology online calculating program (http://ready.arl.noaa.gov/) used in this publication. The speciated AHs emission inventory is provided by Qiang Zhang in Tsinghua University, who is a coauthor of this publication. The measurement data used in this study can be obtained from Yanli Zhang (zhang_yl86@gig.ac.cn) or Xinming Wang (wangxm@gig.ac.cn) upon request.

References

Agency for Toxic Substances and Diseases Registry (ATSDR) (2009), Minimal Risk Levels List, Washington, D. C. [Available at http://www.atsdr.cdc.gov/substances/index.asp.]

Andreae, M. O., and P. Merlet (2001), Emission of trace gases and aerosols from biomass burning, *Global Biogeochem. Cycles*, *15*, 955–966, doi:10.1029/2000GB001382.

Atkinson, R., and J. Arey (2003), Atmospheric degradation of volatile organic compounds, *Chem. Rev.*, *103*, 4605–4638.

Baker, A. K., A. J. Beyersdorf, L. A. Doezema, A. Katzenstein, S. Meinardi, I. J. Simpson, D. R. Blake, and F. S. Rowland (2008), Measurements of nonmethane hydrocarbons in 28 United States cities, *Atmos. Environ.*, *42*(1), 170–182.

Barletta, B., S. Meinardi, F. S. Rowland, C. Y. Chan, X. M. Wang, S. C. Zou, L. Y. Chan, and D. R. Blake (2005), Volatile organic compounds in 43 Chinese cities, *Atmos. Environ.*, *39*, 5979–5990.

Barletta, B., S. Meinardi, I. J. Simpson, S. C. Zou, F. S. Rowland, and D. R. Blake (2008), Ambient mixing ratios of nonmethane hydrocarbons (NMHCs) in two major urban centers of the Pearl River Delta (PRD) region: Guangzhou and Dongguan, *Atmos. Environ.*, *42*, 4393–4408.

Borbon, A., et al. (2013), Emission ratios of anthropogenic volatile organic compounds in northern midlatitude megacities: Observations versus emission inventories in Los Angeles and Paris, *J. Geophys. Res. Atmos.*, *118*, 2041–2057, doi:10.1002/jgrd.50059.

Cai, C. J., F. H. Geng, X. X. Tie, Q. O. Yu, and J. L. An (2010), Characteristics and source apportionment of VOCs measured in Shanghai, China, *Atmos. Environ.*, *44*, 5005–5014.

Carter, W. P. L. (1994), Development of ozone reactivity scales for volatile organic compounds, *J. Air Waste Manage. Assoc.*, *44*, 881–899.

Chan, L. Y., K. W. Chu, S. C. Zou, C. Y. Chan, X. M. Wang, B. Barletta, D. R. Blake, H. Guo, and W. Y. Tsai (2006), Characteristics of nonmethane hydrocarbons (NMHCs) in industrial, industrial-urban, and industrial-suburban atmospheres of the Pearl River Delta (PRD) region of south China, *J. Geophys. Res.*, *111*, D11304, doi:10.1029/2005JD006481.

Chang, C. C., S. J. Lo, J. G. Lo, and J. L. Wang (2003), Analysis of methyl tert-butyl ether in the atmosphere and implications as an exclusive indicator of automobile exhaust, *Atmos. Environ.*, *37*, 4747–4755.

de Gouw, J. A., et al. (2005), Budget of organic carbon in a polluted atmosphere: Results from the New England Air Quality Study in 2002, *J. Geophys. Res.*, *110*, D16305, doi:10.1029/2004JD005623.

Ding, X., X. M. Wang, B. Gao, X. X. Fu, Q. F. He, X. Y. Zhao, J. Z. Yu, and M. Zheng (2012), Tracer-based estimation of secondary organic carbon in the Pearl River Delta, south China, *J. Geophys. Res.*, *117*, D05313, doi:10.1029/02011JD016596.

Ding, X., Q.-F. He, R.-Q. Shen, Q.-Q. Yu, and X.-M. Wang (2014), Spatial distributions of secondary organic aerosols from isoprene, monoterpenes, β-caryophyllene, and aromatics over China during summer, *J. Geophys. Res. Atmos.*, *119*, 11,877–11,891, doi:10.1002/2014JD021748.

Forstner, H. J. L., R. C. Flagan, and J. H. Seinfeld (1997), Secondary organic aerosol from the photooxidation of aromatic hydrocarbons: Molecular composition, *Environ. Sci. Technol.*, *31*, 1345–1358.

Fu, X., S. X. Wang, B. Zhao, J. Xing, Z. Cheng, H. Liu, and J. M. Hao (2013), Emission inventory of primary pollutants and chemical speciation in 2010 for the Yangtze River Delta region China, *Atmos. Environ.*, *70*, 39–50.

Garcia, J. P., S. Beyne-Masclet, G. Mouvier, and P. Masclet (1992), Emissions of volatile organic compounds by coal-fired power stations, *Atmos. Environ.*, *26*(9), 1589–1597.

Guo, H., T. Wang, I. J. Simpson, D. R. Blake, X. M. Yu, Y. H. Kwok, and Y. S. Li (2004), Source contributions to ambient VOCs and CO at a rural site in Eastern China, *Atmos. Environ.*, *38*, 4551–4560.

He, Q., Y. Yan, H. Li, Y. Zhang, L. Chen, and Y. Wang (2015), Characteristics and reactivity of volatile organic compounds from noncoal emission sources in China, *Atmos. Environ.*, *115*, 153–162.

Hu, L., et al. (2015), Emissions of C6-C8 aromatic compounds in the United States: Constraints from tall tower and aircraft measurements, *J. Geophys. Res. Atmos.*, *120*, 826–842, doi:10.1002/2014JD022627.

Huang, C., C. H. Chen, L. Li, Z. Cheng, H. L. Wang, H. Y. Huang, D. G. Streets, Y. J. Wang, G. F. Zhang, and Y. R. Chen (2011), Emission inventory of anthropogenic air pollutants and VOC species in the Yangtze River Delta region, China, *Atmos. Chem. Phys.*, *11*, 4105–4120.

Jaars, K., et al. (2014), Ambient aromatic hydrocarbon measurements at Welgegund, South Africa, *Atmos. Chem. Phys.*, *14*, 7075–7089.

Klimont, Z., D. G. Streets, S. Gupta, J. Cofala, L. X. Fu, and Y. Ichikawa (2002), Anthropogenic emissions of nonmethane volatile organic compounds in China, *Atmos. Environ.*, *36*, 1309–1322.

Kurokawa, J., T. Ohara, T. Morikawa, S. Hanayama, G. Janssens-Maenhout, T. Fukui, K. Kawashima, and H. Akimoto (2013), Emissions of air pollutants and greenhouse gases over Asian regions during 2000–2008: Regional emission inventory in ASia (REAS) version 2, *Atmos. Chem. Phys.*, *13*, 11,019–11,058.

Li, J., S. D. Xie, L. M. Zeng, L. Y. Li, Y. Q. Li, and R. R. Wu (2015), Characterization of ambient volatile organic compounds and their sources in Beijing, before, during, and after Asia-Pacific Economic Cooperation China 2014, *Atmos. Chem. Phys.*, *15*, 7945–7959.

Li, L., et al. (2011), Air quality and emissions in the Yangtze River Delta, China, *Atmos. Chem. Phys.*, *11*(4), 1621–1639.

Li, L., H. Li, X. Zhang, L. Wang, L. Xu, X. Wang, Y. Yu, Y. Zhang, and G. Cao (2014a), Pollution characteristics and health risk assessment of benzene homologues in ambient air in the northeastern urban area of Beijing, China, *J. Environ. Sci.*, *26*, 214–223.

Li, M., et al. (2014b), Mapping Asian anthropogenic emissions of nonmethane volatile organic compounds to multiple chemical mechanisms, *Atmos. Chem. Phys.*, *14*, 5617–5638.

Liu, J. F., Y. J. Mu, Y. J. Zhang, Z. M. Zhang, X. K. Wang, Y. J. Liu, and Z. Q. Sun (2009), Atmospheric levels of BTEX compounds during the 2008 Olympic Games in the urban area of Beijing, *Sci. Total Environ.*, *408*, 109–116.

Liu, Y., M. Shao, L. Fu, S. Lu, L. Zeng, and D. Tang (2008a), Source profiles of volatile organic compounds (VOCs) measured in China: Part I, *Atmos. Environ.*, *42*, 6247–6260.

Liu, Y., M. Shao, S. Lu, C.-c. Liao, J.-L. Wang, and G. Chen (2008b), Volatile organic compound (VOC) measurements in the pearl river delta (PRD) region, China, *Atmos. Chem. Phys.*, *8*, 1531–1545.

Liu, Z., et al. (2012), Exploring the missing source of glyoxal (CHOCHO) over China, *Geophys. Res. Lett.*, *39*, L10812, doi:10.1029/2012GL051645.

Louie, P. K. K., J. W. K. Ho, R. C. W. Tsang, D. R. Blake, A. K. H. Lau, J. Z. Yu, Z. Yuan, X. Wang, M. Shao, and L. Zhong (2013), VOCs and OVOCs distribution and control policy implications in Pearl River Delta region, China, *Atmos. Environ.*, *76*, 125–135.

McCulloch, A., M. L. Aucott, T. E. Graedel, G. Kleiman, P. M. Midgley, and Y.-F. Li (1999), Industrial emissions of trichloroethene, tetrachloroethene, and dichloromethane: Reactive chlorine emissions inventory, *J. Geophys. Res.*, *104*, 8417–8427, doi:10.1029/1999JD900011.

McKeen, S. A., S. C. Liu, E. Y. Hsie, X. Lin, J. D. Bradshaw, S. Smyth, G. L. Gregory, and D. R. Blake (1996), Hydrocarbon ratios during PEM-WEST A: A model perspective, *J. Geophys. Res.*, *101*, 2087–2109, doi:10.1029/95JD02733.

Monod, A., B. C. Sive, P. Avino, T. Chen, D. R. Blake, and F. Sherwood Rowland (2001), Monoaromatic compounds in ambient air of various cities: A focus on correlations between the xylenes and ethylbenzene, *Atmos. Environ.*, *35*, 135–149.

National Bureau of Statistics of China (NBSC) (2013), *China Energy Statistical Yearbook 2013*, China Statistics Press, Beijing.
Nelson, P. F., and S. M. Quigley (1983), The m,p-xylenes:Ethylbenzene ratio. A technique for estimating hydrocarbon age in ambient atmospheres, *Atmos. Environ.*, *17*, 659–662.
O'Dowd, C. D., P. Aalto, K. Hmeri, M. Kulmala, and T. Hoffmann (2002), Aerosol formation: Atmospheric particles from organic vapours, *Nature*, *416*, 497–498.
Odum, J. R., T. P. W. Jungkamp, R. J. Griffin, R. C. Flagan, and J. H. Seinfeld (1997), The atmospheric aerosol-forming potential of whole gasoline vapor, *Science*, *276*, 96–99.
Ou, J., J. Zheng, R. Li, X. Huang, Z. Zhong, L. Zhong, and H. Lin (2015), Speciated OVOC and VOC emission inventories and their implications for reactivity-based ozone control strategy in the Pearl River Delta region, China, *Sci. Total Environ.*, *530–531*, 393–402.
Parrish, D. D., A. Stohl, C. Forster, E. L. Atlas, D. R. Blake, P. D. Goldan, W. C. Kuster, and J. A. de Gouw (2007), Effects of mixing on evolution of hydrocarbon ratios in the troposphere, *J. Geophys. Res.*, *112*, D10S34, doi:10.1029/2006JD007583.
Parrish, D. D., W. C. Kuster, M. Shao, Y. Yokouchi, Y. Kondo, P. D. Goldan, J. A. de Gouw, M. Koike, and T. Shirai (2009), Comparison of air pollutant emissions among mega-cities, *Atmos. Environ.*, *43*, 6435–6441.
Qiu, K., L. Yang, J. Lin, P. Wang, Y. Yang, D. Ye, and L. Wang (2014), Historical industrial emissions of nonmethane volatile organic compounds in China for the period of 1980–2010, *Atmos. Environ.*, *86*, 102–112.
Russell, A., J. Milford, M. S. Bergin, S. McBride, L. McNair, Y. Yang, W. R. Stockwell, and B. Croes (1995), Urban ozone control and atmospheric reactivity of organic gases, *Science*, *269*, 491–495.
Russo, R. S., et al. (2003), Chemical composition of Asian continental outflow over the western Pacific: Results from Transport and Chemical Evolution over the Pacific (TRACE-P), *J. Geophys. Res.*, *108*(D20), 8804, doi:10.1029/2002JD003184.
Sato, K., A. Takami, T. Isozaki, T. Hikida, A. Shimono, and T. Imamura (2010), Mass spectrometric study of secondary organic aerosol formed from the photo-oxidation of aromatic hydrocarbons, *Atmos. Environ.*, *44*, 1080–1087.
Shao, M., B. Wang, S. H. Lu, B. Yuan, and M. Wang (2011), Effects of Beijing Olympics control measures on reducing reactive hydrocarbon species, *Environ. Sci. Technol.*, *45*, 514–519.
Simon, H., et al. (2010), The development and uses of EPA's SPECIATE database, *Atmos. Pollut. Res.*, *1*, 196–206.
Suthawaree, J., S. Kato, K. Okuzawa, Y. Kanaya, P. Pochanart, H. Akimoto, Z. Wang, and Y. Kajii (2010), Measurements of volatile organic compounds in the middle of central East China during Mount Tai Experiment 2006 (MTX2006): Observation of regional background and impact of biomass burning, *Atmos. Chem. Phys.*, *10*, 1269–1285.
Tang, J. H., L. Y. Chan, C. Y. Chan, Y. S. Li, C. C. Chang, S. C. Liu, D. Wu, and Y. D. Li (2007), Characteristics and diurnal variations of NMHCs at urban, suburban, and rural sites in the Pearl River Delta and a remote site in South China, *Atmos. Environ.*, *41*, 8620–8632.
Tang, J. H., L. Y. Chan, C. C. Chang, S. Liu, and Y. S. Li (2009), Characteristics and sources of nonmethane hydrocarbons in background atmospheres of eastern, southwestern, and southern China, *J. Geophys. Res.*, *114*, D03304, doi:10.1029/2008JD010333.
Tang, J. H., K. W. Chu, L. Y. Chan, and Y. J. Chen (2014), Nonmethane hydrocarbon emission profiles from printing and electronic industrial processes and its implications on the ambient atmosphere in the Pearl River Delta, South China, *Atmos. Pollut. Res.*, *5*, 151–160.
Tong, L., X. Liao, J. S. Chen, H. Xiao, L. L. Xu, F. W. Zhang, Z. C. Niu, and J. S. Yu (2013), Pollution characteristics of ambient volatile organic compounds (VOCs) in the southeast coastal cities of China, *Environ. Sci. Pollut. Res.*, *20*, 2603–2615.
Tsai, S. M., J. Zhang, K. R. Smith, Y. Ma, R. A. Rasmussen, and M. A. K. Khalil (2003), Characterization of nonmethane hydrocarbons emitted from various cookstoves used in China, *Environ. Sci. Technol.*, *37*, 2869–2877.
United States Environmental Protection Agency (USEPA) (1995), *Compilation of Air Pollutant Emission Factors (AP42)*, chap. 1, 5th ed., Office of Air Quality Planning And Standards Office of Air And Radiation, U. S. Environmental Protection Agency, Research Triangle Park, North Carolina.
Wang, B., M. Shao, S. H. Lu, B. Yuan, Y. Zhao, M. Wang, S. Q. Zhang, and D. Wu (2010), Variation of ambient nonmethane hydrocarbons in Beijing city in summer 2008, *Atmos. Chem. Phys.*, *10*, 5911–5923.
Wang, H. L., et al. (2013a), Chemical loss of volatile organic compounds and its impact on the source analysis through a 2 year continuous measurement, *Atmos. Environ.*, *80*, 488–498.
Wang, H. L., et al. (2014a), Source profiles and chemical reactivity of volatile organic compounds from solvent use in Shanghai, China, *Aerosol Air Qual. Res*, *14*, 301–310.
Wang, H., Q. Wang, J. Chen, C. Chen, C. Huang, L. Qiao, S. Lou, and J. Lu (2015a), Do vehicular emissions dominate the source of C_6–C_8 aromatics in the megacity Shanghai of eastern China?, *J. Environ. Sci.*, *27*, 290–297.
Wang, M., M. Shao, W. Chen, B. Yuan, S. Lu, Q. Zhang, L. Zeng, and Q. Wang (2014b), A temporally and spatially resolved validation of emission inventories by measurements of ambient volatile organic compounds in Beijing, China, *Atmos. Chem. Phys.*, *14*, 5871–5891.
Wang, M., et al. (2015b), Trends of nonmethane hydrocarbons (NMHC) emissions in Beijing during 2002–2013, *Atmos. Chem. Phys.*, *15*, 1489–1502.
Wang, S. Y., D. W. Wu, X. M. Wang, J. C. H. Fung, and J. Z. Yu (2013b), Relative contributions of secondary organic aerosol formation from toluene, xylenes, isoprene, and monoterpenes in Hong Kong and Guangzhou in the Pearl River Delta, China: An emission-based box modeling study, *J. Geophys. Res. Atmos.*, *118*, 507–519, doi:10.1029/2012JD017985.
Wang, X. M., and T. Wu (2008), Release of isoprene and monoterpenes during the aerobic decomposition of orange wastes from laboratory incubation experiments, *Environ. Sci. Technol.*, *42*, 3265–3270.
Wang, X. M., G. Y. Sheng, J. M. Fu, C. Y. Chan, S. C. Lee, L. Y. Chan, and Z. S. Wang (2002), Urban roadside aromatic hydrocarbons in three cities of the Pearl River Delta, People's Republic of China, *Atmos. Environ.*, *36*, 5141–5148.
Warneke, C., et al. (2007), Determination of urban volatile organic compound emission ratios and comparison with an emissions database, *J. Geophys. Res.*, *112*, D10S47, doi:10.1029/2006JD007930.
Wei, W., S. X. Wang, S. Chatani, Z. Klimont, J. Cofala, and J. M. Hao (2008), Emission and speciation of nonmethane volatile organic compounds from anthropogenic sources in China, *Atmos. Environ.*, *42*, 4976–4988.
Wei, W., S. Wang, J. Hao, and S. Cheng (2014), Trends of chemical speciation profiles of anthropogenic volatile organic compounds emissions in China, 2005–2020, *Front. Environ. Sci. Eng.*, *8*, 27–41.
Xue, L. K., T. Wang, H. Guo, D. R. Blake, J. Tang, X. C. Zhang, S. M. Saunders, and W. X. Wang (2013), Sources and photochemistry of volatile organic compounds in the remote atmosphere of western China: Results from the Mount Waliguan Observatory, *Atmos. Chem. Phys.*, *13*, 8551–8567.
Yan, X., T. Ohara, and H. Akimoto (2006), Bottom-up estimate of biomass burning in mainland China, *Atmos. Environ.*, *40*, 5262–5273.
Yuan, B., M. Shao, S. H. Lu, and B. Wang (2010a), Source profiles of volatile organic compounds associated with solvent use in Beijing, China, *Atmos. Environ.*, *44*, 1919–1926.
Yuan, B., Y. Liu, M. Shao, S. Lu, and D. G. Streets (2010b), Biomass burning contributions to ambient VOCs species at a receptor site in the Pearl River Delta (PRD), China, *Environ. Sci. Technol.*, *44*, 4577–4582.

Yuan, B., W. W. Hu, M. Shao, M. Wang, W. T. Chen, S. H. Lu, L. M. Zeng, and M. Hu (2013), VOC emissions, evolutions and contributions to SOA formation at a receptor site in eastern China, *Atmos. Chem. Phys.*, *13*, 8815–8832.

Zhang, J., Y. Sun, F. Wu, J. Sun, and Y. Wang (2014a), The characteristics, seasonal variation, and source apportionment of VOCs at Gongga Mountain, China, *Atmos. Environ.*, *88*, 297–305.

Zhang, Q., et al. (2009), Asian emissions in 2006 for the NASA INTEX-B mission, *Atmos. Chem. Phys.*, *9*, 5131–5153.

Zhang, Y. J., et al. (2012a), Atmospheric BTEX and carbonyls during summer seasons of 2008–2010 in Beijing, *Atmos. Environ.*, *59*, 186–191.

Zhang, Y. L., et al. (2012b), Aromatic hydrocarbons as ozone precursors before and after outbreak of the 2008 financial crisis in the Pearl River Delta region, south China, *J. Geophys. Res.*, *117*, D15306, doi:10.1029/12011JD017356.

Zhang, Y. L., et al. (2013), Source attributions of hazardous aromatic hydrocarbons in urban, suburban and rural areas in the Pearl River Delta (PRD) region, *J. Hazard. Mater.*, *250*, 403–411.

Zhang, Y., et al. (2014b), Ambient CFCs and HCFC-22 observed concurrently at 84 sites in the Pearl River Delta region during the 2008–2009 grid studies, *J. Geophys. Res. Atmos.*, *119*, 7699–7717, doi:10.1002/2014JD021626.

Zhang, Z., X. Wang, Y. Zhang, S. Lü, Z. Huang, X. Huang, and Y. Wang (2015), Ambient air benzene at background sites in China's most developed coastal regions: Exposure levels, source implications and health risks, *Sci. Total Environ.*, *511*, 792–800.

Zhao, L., X. Wang, Q. He, H. Wang, G. Sheng, L. Y. Chan, J. Fu, and D. R. Blake (2004), Exposure to hazardous volatile organic compounds, PM_{10} and CO while walking along streets in urban Guangzhou, China, *Atmos. Environ.*, *38*, 6177–6184.

Zheng, J. Y., M. Shao, W. W. Che, L. J. Zhang, L. J. Zhong, Y. H. Zhang, and D. Streets (2009), Speciated VOC emission inventory and spatial patterns of ozone formation potential in the Pearl River Delta, China, *Environ. Sci. Technol.*, *43*, 8580–8586.

Zheng, J., Y. Yu, Z. Mo, Z. Zhang, X. Wang, S. Yin, K. Peng, Y. Yang, X. Feng, and H. Cai (2013), Industrial sector-based volatile organic compound (VOC) source profiles measured in manufacturing facilities in the Pearl River Delta, China, *Sci. Total Environ.*, *456–457*, 127–136.

Zong, Z., X. Wang, C. Tian, Y. Chen, L. Qu, L. Ji, G. Zhi, J. Li, and G. Zhang (2016), Biomass burning contribution to regional $PM_{2.5}$ during winter in the North China, *Atmos. Chem. Phys. Discuss.*, *16*, 1–41.

Zou, Y., et al. (2015), Characteristics of 1 year of observational data of VOCs, NOx and O3 at a suburban site in Guangzhou, China, *Atmos. Chem. Phys.*, *15*, 6625–6636.